Shear Banding Fluctuations and Nematic Order in Wormlike Micelles

M. R. López-González,[1] W. M. Holmes,[1] P. T. Callaghan,[1] and P. J. Photinos[2]

[1]*MacDiarmid Institute for Advanced Materials and Nanotechnology, School of Chemical and Physical Sciences, Victoria University of Wellington, New Zealand*

[2]*Department of Physics, University of Southern Oregon, Ashland, Oregon 97520, USA*

(Received 15 August 2004; published 20 December 2004)

Using rapid NMR velocimetry we demonstrate the existence of shear band fluctuations in the Couette flow of the wormlike micelle system, 10% w/v cetylpyridinium chloride and sodium salicylate (molar ratio 2:1) in 0.5 M ^2H_2O NaCl brine. We show that the fluctuations may be either quasirandom or periodic, the fluctuation spectrum being similar to that observed in the stress. Despite the equilibrium fluid being far from an isotropic-nematic transition, deuterium NMR shows that the onset of shear banding is associated with a nematic micellar state whose order parameter depends on shear rate.

DOI: 10.1103/PhysRevLett.93.268302 PACS numbers: 83.80.Qr, 82.70.Uv, 83.60.Pq, 83.60.Wc

Shear banding is associated with complex fluids that exhibit inherent double-valuedness in the underlying flow curve (stress versus strain rate) [1]. Above a critical average (apparent) strain rate, such systems may separate into coexisting phases [2] for which local strain rates widely differ, despite a common stress. A consequent rheomechanical feature is the existence of a stress plateau over a wide strain-rate range, canonical examples being provided by semidilute wormlike micelles [3], systems for which dissociation-recombination reactions [4] play a role in the chain dynamics. Shear banding in wormlike micelles has been observed through direct velocimetry [5–7], and in some cases, banding has been associated with birefringence effects [8–10], suggesting the possibility of nematic ordering. However, in most measurements where shear banding is believed to occur, fluctuations are common [10–16], a phenomenon which has presented a challenge for theory.

The simple picture of shear banding has been that the spatially distinct bands reside, at a coexistence stress [17], on stable branches of the flow curve, thus allowing a steady-state solution to the equations of motion. However, in a recent paper, Fielding and Olmsted [18] predicted that systems exhibiting shear banding could manifest complex fluctuation dynamics [19]. Their model shows that a coupling between flow and microstructure has the effect of destabilizing the high shear rate band and suggests that both spatio-temporal oscillations and chaotic banded flows are possible, depending on small changes in the model parameters. The chosen coupled variable was the micellar length. While this is a natural choice in the case of wormlike micelles, these authors pointed out that almost any microstructural property would suffice. For example, Rienecker *et al.* have considered the interplay between flow and isotropic-nematic microstructure [20] in influencing rheo-chaos. Fielding and Olmsted use a double-valued constitutive relation $g[\dot{\gamma}\tau(n)]$ in which the characteristic length, $\tau(n)$, depends on local micelle length, n, while the steady (homogeneous) state micelle length, $N(\dot{\gamma}\tau_n)$, is shear-dependent either through flow enhanced scission (N decreases) or through enhanced recombination associated with shear-induced alignment (N increases) [21].

Recently, ultrasound measurements have been used to observe velocity profile fluctuations in a wormlike micelle system close to an isotropic-nematic (IN) transition [22]. We present here an experimental study of fluctuations in shear-banded flow for a wormlike micelle system far from the IN transition. We measure not only the locally fluctuating velocity profiles, but also the micellar order parameter. Our data show that indeed the micelle properties are coupled to strain rate. Further, in the same system, under nearly identical conditions, we are able to observe both strongly oscillatory fluctuations as well as those comprising quasirandom character.

The micellar system chosen here, 10% w/v cetylpyridinium chloride and sodium salicylate (molar ratio 2:1) in 0.5 M H_2O NaCl brine, exhibits a flow curve with a wide

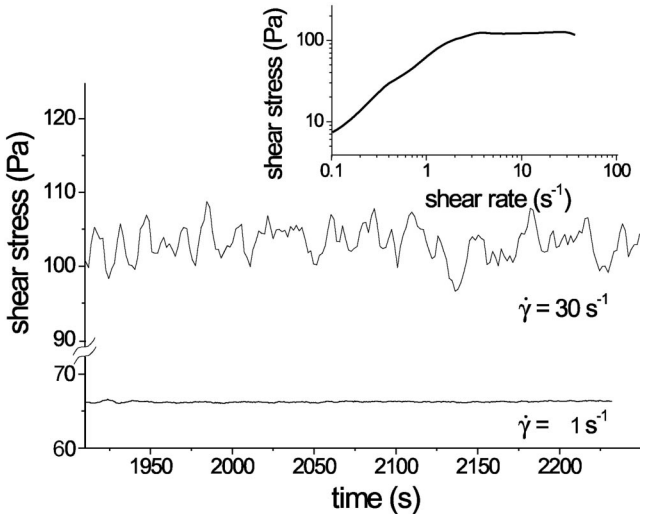

FIG. 1. Stress fluctuations, measured on the plateau at 30 s^{-1}, in cone-and-plate geometry for the wormlike micelle system. The inset shows the flow curve measured under controlled strain rate.

stress plateau [9]. Linear viscoelastic measurements give a plateau modulus of 252 Pa and a Maxwell time of 0.46 s. Note that the IN transition occurs at the much higher concentration of 30% w/v [9]. Figure 1 shows the flow curve obtained at 25 C on a strain-rate controlled Rheometrics ARES rheometer using a 40 mm diameter, 0.04 rad cone-and-plate geometry, for which the strain-rate sweep had a residence time of 30 s per point. The figure also shows that the stress measured at a point on the plateau ($\dot{\gamma} = 30\ s^{-1}$) exhibits strong fluctuations while that measured in the Newtonian region is approximately constant within the instrument precision ($\sim 1\%$).

Our NMR experiment is performed using a cylindrical cell made of the hard polymer, PolyEtherEtherKetone (PEEK), with inner and outer wall radii of 8.5 mm and 9.5 mm, respectively. The inner wall is serrated (~ 0.02 mm) to help suppress any tendency to slip. In an earlier NMR study [15], we used Fourier phase encoding [23] to measure the distribution of velocities, $P(v)$, at 13 pixels spanning the gap, the total time for the experiments being around four hours. These distributions indicated that velocity fluctuations were present, although, because of the long time taken to average, we were unable to ascertain the temporal structure. By taking an entirely different approach, we are able to increase our imaging speed by $\sim 10^4$, permitting NMR velocimetry at 1 s resolution. Our method is based on the RARE (rapid acquisition with relaxation enhancement) sequence [24] and our speed advantage is gained by using a single phase encoding step for the velocity and a single acquisition instead of signal averaging. Furthermore, by utilizing the efficiency gain of a multiecho train to encode for position along the flow direction, we are able to image in two dimensions over a limited sector field of view ($\nabla \mathbf{v}$ direction, 50 pixels, 5 mm) $\times$ ($\mathbf{v}$ direction, 32 pixels, 25 mm) including the Couette cell gap. The price paid for this speed increase, in addition to a small sacrifice of spatial resolution, is that we are no longer able to measure the velocity distribution in each pixel, only its average value over the phase encode time of $\Delta = 10$ ms. However, because the fluctuation time is longer than the image repetition time of 1 s, such an average provides a real time glimpse of the instantaneous velocity profiles. Further, because we are able to image the spatial extent of that profile along the flow direction, we are able to ascertain the extent to which fluctuations are spatially correlated. Note that our measurement does involve an average along the vorticity ($\nabla \times \mathbf{v}$) axis over 5 mm.

Figure 2(a) shows a set of 512 velocity profiles taken at 1 s intervals from a 780 μm wide slice across the 1 mm gap, as shown schematically in Fig. 2(b). Figure 2(b) also shows the result of 64 separate profiles, while Fig. 2(c) shows randomly selected profiles superposed. Fluctuations are clearly visible, with velocity at the inner wall distinctly smaller than the wall velocity of 37 mm s^{-1}, indicating slip. One intriguing aspect of the fluctuations is that they seem to be driven by the slip at the inner wall. While the fluid does separate into two bands of, respectively, higher and lower shear rates, the high shear rate band exhibits a consistent value of around 70 s^{-1}, but the extent of the band is determined by the degree of slip. This observation is consistent with the model used to explain velocity distributions found in our time-averaged measurements [15] and the histogram of velocities at each position found using rapid velocimetry closely matches those earlier data.

The time-dependent velocity profiles observed here have obvious spatial and temporal coherence. In particular, we note that along the extra dimension of the velocity axis (not shown), we found a uniform profile, indicating that the correlation length was ≥ 5 mm, the range over which we were able to encode for velocity without perturbation from the cell curvature. The temporal correlation can be ascertained by calculating the velocity autocorrelation function (VACF) and its Fourier spectrum at various pixels across the cell. Figure 3(a) shows the result for pixel 3 (a similar spectrum was found at all positions). Initial correlation is

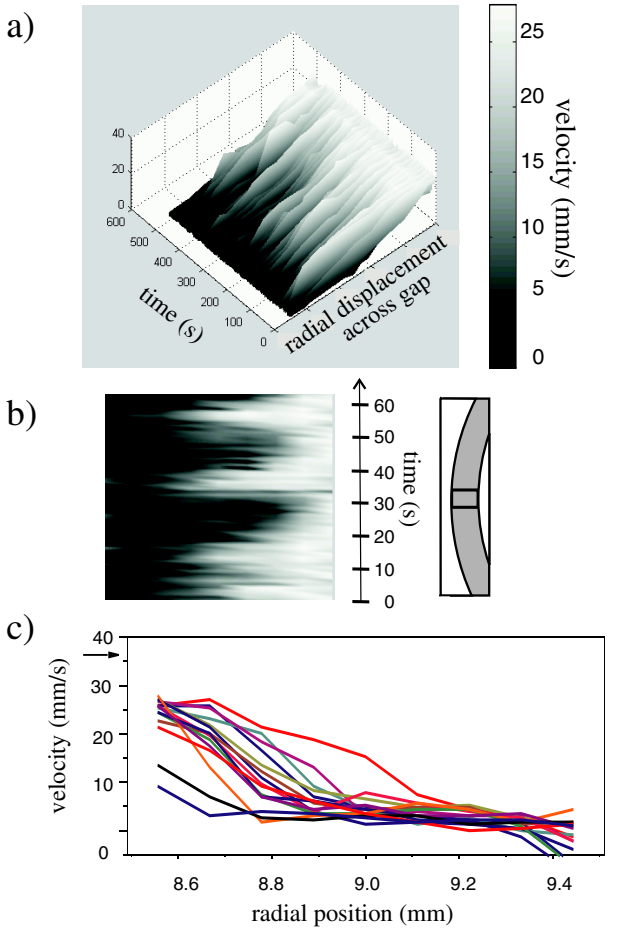

FIG. 2 (color online). (a) Velocity profiles across the 1 mm gap at successive 1 s intervals of the cylindrical Couette cell at apparent shear rate 37 s^{-1}. The layer (~ 50 μm) nearest the inner wall cannot be resolved. (b) A 64 s section. (c) The superposition of a random selection of profiles in which the degree of slip is seen to correlate with the width of the shear band.

strongly damped after 10 s, although the VACF exhibits some oscillatory character, as apparent in the spectral density in the band 0.04 to 0.06 Hz. Note that these frequencies are significantly lower than the rotation frequency of 0.6 Hz, and further, that the correlation time of order 10 s is similar to that seen in the stress fluctuations. Remarkably, the nature of the velocity fluctuations is highly sensitive to sample preparation. The behavior exhibited in Fig. 3(a) was found consistently with one batch of material (Aldrich), but a fresh sample formed from a new batch of surfactant manifested the strong oscillatory behavior of Fig. 3(b). We note previously observed [11] dependence of shear-banding fluctuations on supplier and batch number.

While NMR can be used to image velocity, its advantage lies in its use as a spectroscopic tool, revealing properties at the molecular scale. We have investigated the micelles during the shear-banding fluctuations by using deuterium magnetic resonance to measure micellar order. For deuterons (spin quantum number $I = 1$) there may exist a quadrupolar interaction which is detected as a first order perturbation projected into the dominant Zeeman representation as [25]

$$H_Q(t) = AP_2[\cos(\theta(t))][3I_z^2 - I(I+1)], \qquad (1)$$

the interaction strength parameter, A, being determined by the nuclear spin properties and the details of the electronic environment (the molecular bond containing the deuteron). P_2 is the second Legendre polynomial and $\theta(t)$ describes the fluctuating orientation (with respect to the magnetic field direction) of the bond direction. Provided that this motion is fast compared with A, the Legendre polynomial is motionally averaged to its mean, and, where a hierarchy of anisotropic motion exists, each step projects a $\langle P_2 \rangle$ factor in a product of such terms. At the final stage, one senses the mesophase Saupe order parameter, S_{zz}, although its absolute value must be deduced by comparison with a known phase. Note that the effect of the quadupole interaction is to split the deuterium NMR spectrum such that the doublet separation is proportional to S_{zz}.

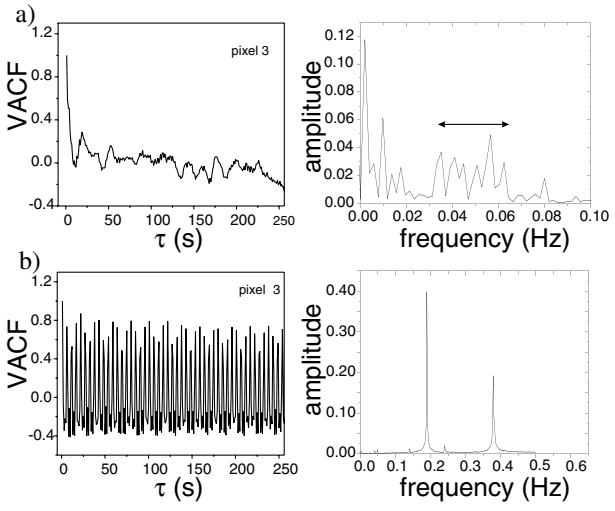

FIG. 3. Velocity autocorrelation functions at 37 s^{-1} and spectral densities for velocities measured at pixel 3, 0.3 mm from the inner wall for two different batch preparations of wormlike micelle (a), (b).

Here we introduce the deuteron both by deuterating the water solvent, and by introducing, into the micelles, a dilute (1% w/v) deuterated decane probe molecule. The former method has the advantage of high signal amplitude, permitting us to image the spectrum across the 1 mm gap. However, it suffers from being only weakly sensitive to micelle orientation through an indirect motional averaging process as water molecules occasionally collide with the micelles. By contrast, the latter method is strongly sensitive to micellar orientation due to the intimate contact acquired by the probe molecule, but the low signal strength means that only gap-averaged spectra are able to be acquired.

The ^2H_2O deuterium NMR spin echo signal was obtained using a spectroscopic imaging pulse sequence which allows us to reconstruct the NMR spectrum at 70 μm intervals across the 1 mm gap, as shown in Fig. 4(a) [26]. The quadrupole interaction is too weak to produce a spectral splitting but noticeable broadening correlates with the region of the high shear band. By contrast, no broadening is evident at the lower shear rates. If we interpret the strength of the quadrupole interaction as reflecting the degree of micellar order, then for a static shear band structure, one might expect a sudden transition from broad to narrow lines at the band interface. By contrast, we observe a broadening which gradually decreases with increasing radial displacement from the inner wall, an observation consistent with the radial fluctuations in the band interface apparent in Fig. 2. Note that the time scale associated with signal acquisition ($\sim$1 s) is much shorter than the fluctuation time seen in Fig. 2. However, in order to obtain an image, averaging was performed over several hours.

The deuterated decane spectrum, arising from the signal integral across the gap shows, at zero shear, a single peak that we associate with an isotropic phase. However, once the critical shear rate (3 s^{-1}) is exceeded, a second phase with strong quadrupole splitting ($\sim$2 kHz) appears, as seen in Fig. 4(b). This signal provides clear indication that the high shear rate band is associated with a nematic state. Independent measurements of the splitting, at zero shear, for the same wormlike micelle system at higher concentrations (40%) in its nematic phase, indicate that the shear-induced nematic state seen in Fig. 4(b) has a micellar order parameter close to unity. We note that the proportion, x, of the induced nematic phase increases with increasing apparent shear rate, $\dot{\gamma}$, an effect we might associate with the usual lever rule, $\dot{\gamma} = (1-x)\dot{\gamma}_L + x\dot{\gamma}_H$, the high and low shear rate bands being described by $\dot{\gamma}_H$ and $\dot{\gamma}_L$, respectively. Surprisingly, the size of the quadrupole splitting also increases markedly with increasing $\dot{\gamma}$, suggesting that the

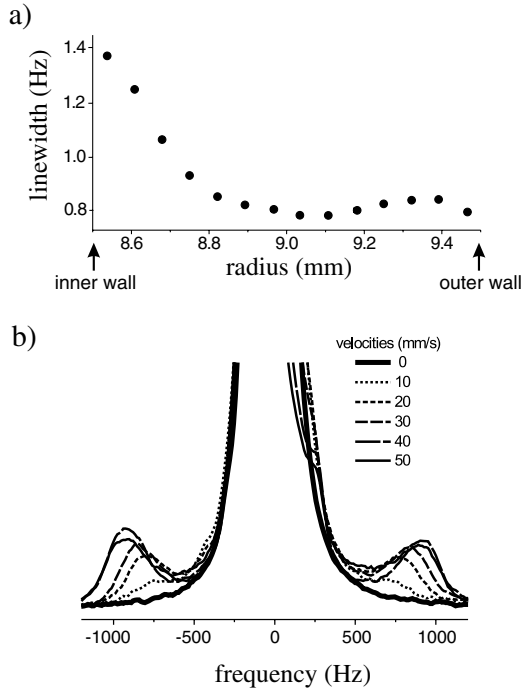

FIG. 4. (a) Homogeneous linewidth of the ^2H_2O deuterium NMR signal at 37 s^{-1} as a function of gap radial displacement, and (b) deuterium NMR spectrum obtained from decane molecules partitioned within the micelles. Note the splitting that arises from an oriented phase while the central line arises from the isotropic phase.

micellar order for fluid resident on the high shear band is itself a function of the average gap shear rate. This finding is reminiscent of the Fielding-Olmsted picture, where the micellar length depends on the local $\dot{\gamma}$. Fortunately, shear band fluctuations are too slow to motionally average the $\sim$2 kHz quadrupole interaction, so that the gap-averaged contributions to the isotropic and nematic spectral features are properly resolved without perturbation to the spectral shape.

The results presented here provide clear evidence, not only for the existence of slow fluctuations in shear band structure, but also for the existence of a high degree of nematic order in the high shear band phase, despite the equilibrium fluid being far from an IN transition. Further, we observe either quasirandom or strongly periodic fluctuation modes on subtle changes to the material preparation. While we have not yet achieved a time resolution in our spectroscopic measurements sufficient to correlate fluctuations in velocity and nematicity, we attach some significance to the observation of a dependence of order parameter on shear rate. This cannot be explained by the simple, steady-state, two fluid model, and suggests a coupling between the hydrodynamic flow and the microscopic details of the micellar structure. To our knowledge, this represents the first such demonstration of a connection between shear band instability and flow-microstructure coupling.

The authors are grateful to Dr. Suzanne Fielding and Dr. Peter Olmsted for valuable discussions. We also acknowledge financial support from the Royal Society of New Zealand Marsden Fund and Centres of Research Excellence Fund.

[1] T. C. B. McLeish and R. C. Ball, J. Polym. Sci. Polym. Phys. B **24**, 1735 (1986).
[2] M. E. Cates, T. C. B. McLeish, and G. Marrucci, Europhys. Lett. **21**, 451 (1993).
[3] H. Rehage and H. Hoffman, Mol. Phys. **74**, 993 (1991).
[4] M. E. Cates, J. Phys. Chem. **94**, 371 (1990).
[5] R. W. Mair and P. T. Callaghan, Europhys. Lett. **36**, 719 (1996).
[6] M. M. Britton and P. T. Callaghan, Phys. Rev. Lett. **78**, 4930 (1997).
[7] E. Fischer and P. T. Callaghan, Phys. Rev. E **64**, 011501 (1990).
[8] R. Makhloufi, J.-P. Decruppe, A. Aït-Ali, and R. Cressely, Europhys. Lett. **32**, 253 (1995).
[9] J.-F. Berret, G. Porte, and J.-P. Decruppe, Phys. Rev. E **55**, 1668 (1997); J.-F. Berret, D. Roux, and G. Porte, J. Phys. II (France) **4**, 1261 (1994).
[10] P. Fischer, Rheol. Acta **39**, 234 (2000).
[11] M. M. Britton and P. T. Callaghan, Eur. Phys. J. B **7**, 237 (1999).
[12] P. Fischer, E. K. Wheeler, and G. G. Fuller, Rheol. Acta **41**, 35 (2002).
[13] A. F. Méndez-Sánchez, M. R. López-González, V. H. Rolón-Garrido, J. Pérez-González, and L. de Vargas, Rheol. Acta **42**, 56 (2003).
[14] M. E. Cates, D. A. Head, and A. Ajdari, Phys. Rev. E **66**, 025202 (2002).
[15] W. M. Holmes, M. R. López-González, and P. T. Callaghan, Europhys. Lett. **64**, 274 (2003).
[16] R. Bandyopadhyay, G. Basappa, and A. K. Sood, Phys. Rev. Lett. **84**, 2022 (2000).
[17] P. D. Olmsted and C-Y. D. Lu Phys. Rev. E **60**, 4397 (1999).
[18] S. M. Fielding and P. D. Olmsted, Phys. Rev. Lett. **92**, 084502 (2004).
[19] S. M. Fielding and P. D. Olmsted, Eur. Phys. J. E **11**, 65 (2003).
[20] G. Rienacker, A. Kroger, and S. Hess, Phys. Rev. E **66**, 040702 (2002).
[21] M. E. Cates and M. S. Turner, J. Phys. Condens. Matter **4**, 3719 (1992).
[22] L. Becu, S. Manneville, and A. Colin, Phys. Rev. Lett. **93**, 018301 (2004).
[23] P. T.Callaghan, *Principles of Magnetic Resonance Microscopy* (Oxford University, New York, 1991).
[24] J. Hennig, A. Nauerth, and H. Friedburg, Magn. Reson. Med. **3**, 823 (1986).
[25] C. P. Slichter, *Principles of Magnetic Resonance* (Springer, New York, 1996).
[26] W. M. Holmes, M. R. López-González, and P. T. Callaghan, Europhys. Lett. **66**, 132 (2004).